Programme Area: Carbon Capture and Storage

Project: Storage Appraisal

Title: Interjectivity Related Geomechanical Modelling of Large Open Aquifer

Abstract:

This document is a supporting document to deliverable MS6.1 UK Storage Appraisal Final Report.

Context:

This £4m project produced the UK's first carbon dioxide storage appraisal database enabling more informed decisions on the economics of CO2 storage opportunities. It was delivered by a consortium of partners from across academia and industry - LR Senergy Limited, BGS, the Scottish Centre for Carbon Storage (University of Edinburgh, Heriot-Watt University), Durham University, GeoPressure Technology Ltd, Geospatial Research Ltd, Imperial College London, RPS Energy and Element Energy Ltd. The outputs were licensed to The Crown Estate and the British Geological Survey (BGS) who have hosted and further developed an online database of mapped UK offshore carbon dioxide storage capacity. This is publically available under the name CO2 Stored. It can be accessed via www.co2stored.co.uk.

UKSAP

Appendix A5.8

Injectivity Related Geomechanical Modelling of Large Open Aquifers

Conducted for

The Energy Technologies Institute

By

Heriot-Watt University

Author	Peter Olden
Technical Audit	Gillian Pickup
Quality Audit	
Release to Client	Grahame Smith
Date Released	28th October 2011 (final)

File Location
Appendix A5.8 - Injectivity Related Geomechanical Modelling of Large Open Aquifers.doc

Executive Summary

This report primarily describes the development of coupled geomechanical reservoir simulation models undertaken as part of Work Package 4: Dynamical Modelling of the UK Storage Appraisal Project. The work was focused on the modelling of large open aquifers (LOAs) and carried out in two parts. The first part looked at representative structures (generic models) of low injectivity LOAs and the second part on the specific Exemplar 1 (Forties) aquifer. One of the objectives of the geomechanical modelling work was to see if there was any scope for changing the maximum injection pressures from those based on fracture pressure gradient to some other geomechanical criterion. A supplementary (non-geomechanical) study looked at the sensitivity of total CO_2 injected to the magnitude of the fracture pressure gradient assumed. The general conclusion from the work was that maximum injection pressures based on fracture pressure gradient were conservative and should generally be used for storage assessment in the project.

Contents

List of Tables

List of Figures

1 Introduction

When CO_2 is injected into a porous and permeable formation, it will be forced into pores at a higher pressure than the surrounding rock. This causes changes to the stress state of the rock mass which leads to deformation and possible failure of the reservoir and/or seal rock. Pre-existing fractures or faults may be opened up and/or new fractures or faults created, potentially providing conduits for leakage. The conditions under which this may happen are site specific and depend on the injection pressures utilised, the characteristics of the host formation, the in situ stress regime and, in the case of a hydrocarbon reservoir, the production history.

The most immediate risk to leakage in CO_2 geological storage is posed by breaching the caprock. As injection progresses the storage formation pressure increases and the caprock may be subjected to hydraulic fracturing and/or shear failure. These modes of rock failure may provide openings through the reservoir seal allowing contained fluids to migrate to other formations. The shear failure may be manifested by the creation of new fractures or the reactivation of pre-existing faults. Reactivation may also take place on faults within and transecting the reservoir.

It should be noted that deleterious geomechanical effects may take place in locations either associated or not directly associated with the CO_2 migration pathways so it is important to be able to predict both the fluid flow and geomechanical behaviour. Some effects may not necessarily pose risks to storage integrity. However, the question of maximum injection rate which is directly related to the maximum injection pressure in the well, can induce hydraulic fracturing at the wellbore and it therefore also a geomechanical issue.

Although reservoir simulation is a well established tool in the exploitation of hydrocarbon reservoirs, geomechanical modelling is less practised. In the past, reservoir geomechanics was not considered a priority, with many reservoirs considered technically straight-forward and having undergone only limited depletion and/or pressure support. However, declining resource volumes and increasing oil prices have prompted operators to seek less accessible prospects in formations with higher pressures, higher temperatures and in potentially tectonically active regions. Failure to appreciate the importance of geomechanics in these circumstances can have severe consequences in terms of compaction, subsidence, wellbore stability, fault reactivation etc. The topic of CO_2 geological storage brings a new set problems to this field.

There are various approaches to reservoir simulation incorporating geomechanical effects. A coupled analysis whereby there is feedback from the geomechanical model to the flow model is now considered the preferred method. The stress and strain state of the geomechanical model is used to modify the hydraulic properties (porosity and permeability) of the flow model according to (usually) empirical relationships. The exchange of data between the two simulations can be scheduled to take place at different times according to the magnitude of say the pore pressure changes taking place. A fully coupled analysis all conducted within the same code in which the flow and deformation calculations are solved simultaneously is the most rigorous type of simulation but there may be a heavy computational requirement. The VISAGE (Schlumberger, 2009) system used in the work reported here uses the former method.

2 Generic Geomechanical Modelling: Large Open Aquifers

2.1 Introduction

This work was undertaken to support Representative Structure calculations specifically for RS grids with low permeability large open aquifers, in which low capacities had been identified (RPS Energy, 2011). This work confirmed the low capacities calculated, based on limited injectivity and risk of geomechanical failure.

2.2 Development of Reservoir Simulation Models

The reservoir simulation models of CO_2 low injectivity large open aquifers were developed using the ECLIPSE 100 black oil simulator wherein the water phase is modelled as oil. The grids for the aquifer models were constructed using varying areal grid spacing, refined at a horizontal well location and coarsened to the model boundaries. The models all covered the same areal extent – 10 km × 6 km, with the well located on one long edge. By symmetry considerations only one half of the represented domain was treated i.e. the well was 500 m in length, representing a 1 km long well.

Since only the pressure response of the aquifer system is of importance for geomechanical effects, the dip of the aquifers (which affects CO_2 migration) was neglected and all the models were treated as horizontal. The thickness of model layers was refined at the well location, coarsening to the model top and bottom boundaries. The layer thicknesses in the vicinity of the well were kept the same for all models, except for Unit 205 (Alness_012) which had a very low gross thickness. Additional layers of increasing thickness out to the model boundaries were added to make up the overall varying gross thickness of the models. The layers were also set so that the well was located at a datum corresponding to the centroid depth of 80% of the gross aquifer thickness below the aquifer top surface.

An example of the model grid is shown in **Figure A2.1**. This figure – where the porosity property has been plotted – also shows how the boundary of the model has been treated to represent the extent of the aquifer. In the absence of other data, each aquifer was assumed to have a total area of 5000 km^2 (2500 km^2 half model). The cells on the "exterior" vertical boundaries then had a porosity multiplier applied so that the total pore volume of the model was equivalent to that as if the model extended to the above total area. The other grid property data (permeability and net-to-gross) for the models was taken as given in **Table A2.1**. Horizontal permeabilities were taken to be isotropic, but a k_v/k_h ratio of 0.1 was assumed. The additional derived grid data is given in **Table A2.2**.

Aquifer name	Unit No.	Permeability (mD)	Dip (°)	Net thickness (m)	Gross thickness (m)	Vertical NTG	Porosity	Centroid depth (mTVDSS)
Findhorn	174	5	2.5	421	495	0.85	0.19	2635
Lossiehead	19	5	3.3	226	283	0.8	0.13	2105
Hopeman_012	71	5	3.7	109	109	1.0	0.15	2156
Orcadia_013	168	10	5.7	76	380	0.2	0.06	1213
Alness_012	205	1	4.5	32	38	0.85	0.25	2847

Table A2.1: General specification of low injectivity large open aquifers

Unit No.	Porosity	Edge porosity multiplier	Top depth (m)
174	0.19	62.0033	2239.0
19	0.13	42.4233	1878.6
71	0.15	48.9500	2068.8
168	0.06	19.5800	909.0
205	0.25	81.5833	2816.6

Table A2.2: Additional grid properties of low injectivity large open aquifer models

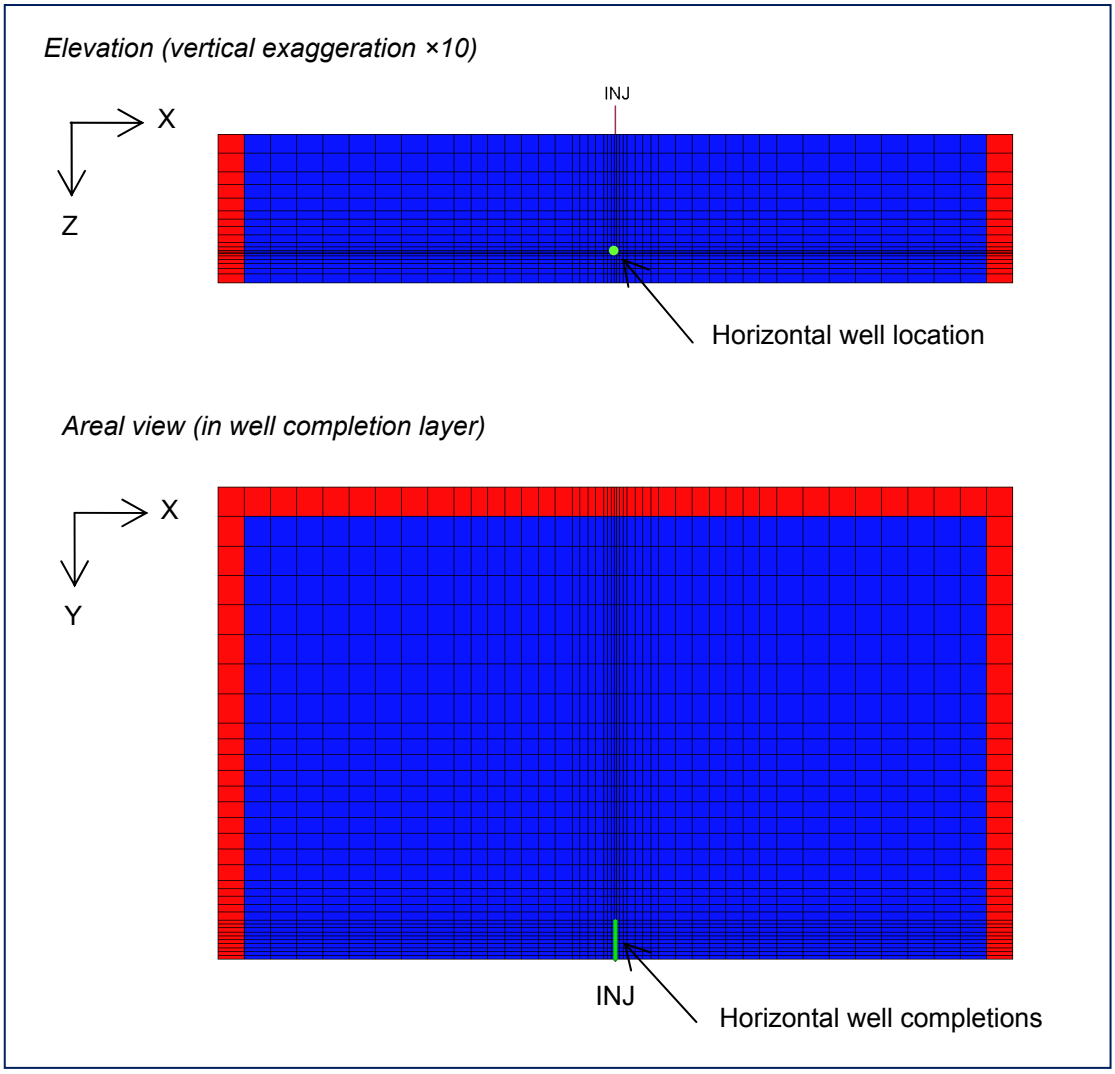

Figure A2.1: General appearance of model grid showing porosity distribution. Blue colour is "normal" porosity, red colour indicates porosity multiplier applied to edge cells

ECLIPSE 100 PVT fluid data for the models were downloaded from the UKSAP sharepoint website. This data covers modelled fluid data for a range of brine salinities and temperatures. A brine salinity of 100,000 ppm was assumed for all the models, corresponding to a brine density of 1067.272805 kg/m^3, which together with an assumed atmospheric pressure of 1.013 bar, enabled reference pressures at datum depths to be calculated for each aquifer. In addition, using an assumed geothermal gradient of 5°C + 25 deg C/km, the aquifer temperatures were calculated to the nearest 5°C. These data are presented in **Table A2.3** and enabled an appropriate set of PVT data to be selected from the sharepoint data, to be incorporated into the model input.

Unit No.	Datum depth (m)	Aquifer pressure[1] (bar)	Aquifer temperature[2] (°C)	Rounded to nearest 5°C (°C)
174	2635	276.9	70.9	70
19	2105	221.4	57.6	60
71	2156	226.7	58.9	60
168	1213	128.0	35.3	35
205	2847	299.1	76.2	75

Table A2.3: Assumed aquifer pressure and temperature data

Relative permeability and capillary pressure data were also downloaded from the sharepoint website. The Viking1 dataset (low permeability) was utilized for all models. The ECLIPSE input data of the models was checked for integrity using a CO_2 injection rate of 1 Mt/year[3] through a horizontal interval of 10 cells for a period of 50 years, with restart files generated at annual timesteps.

2.3 Development of Geomechanical Models

Once the ECLIPSE 100 models were running satisfactorily, the input data was imported into VISAGE Modeler, to prepare the geomechanical models of the aquifers. The geomechanical models were "edited" in Modeler without embedding i.e. the addition of over-, under- or side-burden. This considerably reduced the complexity of the models. For the purposes of geomechanical modelling the aquifers were assumed to be composed of a single homogenous material. The elastic and non-linear properties of this material are given in **Table A2.4**. In the absence of any other information about the geomechanical properties of the aquifer, generic sandstone rock type data was used. A Mohr-Coulomb failure criterion was chosen with a conservative cohesion value of 100 kPa.

2.3.1 Stress Initialisation

A VISAGE geomechanical analysis calculates effective stresses, where the effective stress is the total stress minus the pore pressure. In a coupled ECLIPSE/VISAGE analysis the pore pressure changes calculated by ECLIPSE are used to modify the stresses starting from an initial effective stress state that must be set up in VISAGE. The simplest method of stress initialisation was used for the aquifer models whereby the initial stress state is specified or "wished" into place, rather than being induced by external pressures and reaction forces.

The vertical effective stresses were set with a total stress gradient of 22.44 kPa/m and a pore pressure gradient of 10.0 kPa/m. Using this method, for the purposes of the coupled geomechanical analysis with ECLIPSE, the absolute value of these gradients is not strictly important. It is the difference in these gradients which determines the initial effective stress gradient, which in this case will be 12.44 kPa/m (0.55 psi/ft). The horizontal total stress coefficients (maximum and minimum) were taken to be identical with a value of 0.7228, which corresponds to an effective stress ratio of 0.5.

[1] Assuming aquifer brine salinity 100,000 ppm NaCl
[2] Assuming geothermal gradient 5°C + 25 deg C/km
[3] "Half model equivalent", 728,152 sm^3/day, assuming a CO_2 surface density of 1.88 kg/m^3.

Geomechanical property	Value
Elastic	
Young's modulus GPa	2.0
Poisson's ratio	0.2
Biot's coefficient	1.0
Non-linear	
Mohr-Coulomb failure criterion	
Cohesion kPa	100
Angle of internal friction °	30
Dilation angle°	5
Tensile cut-off kPa	~∞
Fluidity parameter	1.0
Hardening parameter	0.0
Initialisation	
Total vertical stress gradient kPa/m	22.44
Additional vertical stress kPa	0.0
Maximum horizontal stress coefficient	0.7228
Minimum horizontal stress coefficient	0.7228
Horizontal stress azimuth°	0.0
Vertical stress inclination°	90.0
Pore pressure gradient kPa/m	10.0
Additional pore pressure kPa	0.0

Table A2.4: Assumed aquifer geomechanical properties

2.3.2 Failure Assessment

The ECLIPSE 100 model of each aquifer was run coupled to VISAGE without porosity or permeability updating i.e. so that the pressure changes from the ECLIPSE simulation were only used to modify the stress/strain state through changes in effective stress, and there was no feedback to the flow model. Coupling timesteps of 1 year interval were chosen. The ECLIPSE simulation was run with a particular CO_2 injection rate and the resulting VISAGE simulation reviewed to see if any regions of the geomechanical model had failed. Failure is illustrated by reference to **Figure A2.2**.

Fracturing of the intact rock can be analysed directly in VISAGE by examining a property termed the "failure value" available in Modeler. This property is a measure of the proximity of the stress state at a particular location to the failure envelope. The failure value is a large negative number when the stress state is remote from the failure envelope and becomes less negative the closer the stress state is to the failure envelope. At failure the value is zero. A typical plot failure value for one of the aquifer models is shown in **Figure A2.3**.

The procedure to assess the aquifers was to run the models by trial and error with varying injection rates. If failure was detected, the injection rate was reduced and then run again. Conversely if failure was not detected the injection rate was increased. This was repeated until two cases could be identified, one for which failure just occurred and one for which it was just about to. The latter case was then noted as the maximum injection rate. Obviously it would have been necessary to repeat this process to get greater accuracy, but usually only 5

or 6 runs were necessary to achieve a value to 2 significant figures. The maximum injection rates determined for the aquifer models is given in **Table A2.5**, together with the total CO_2 injected in 50 years.

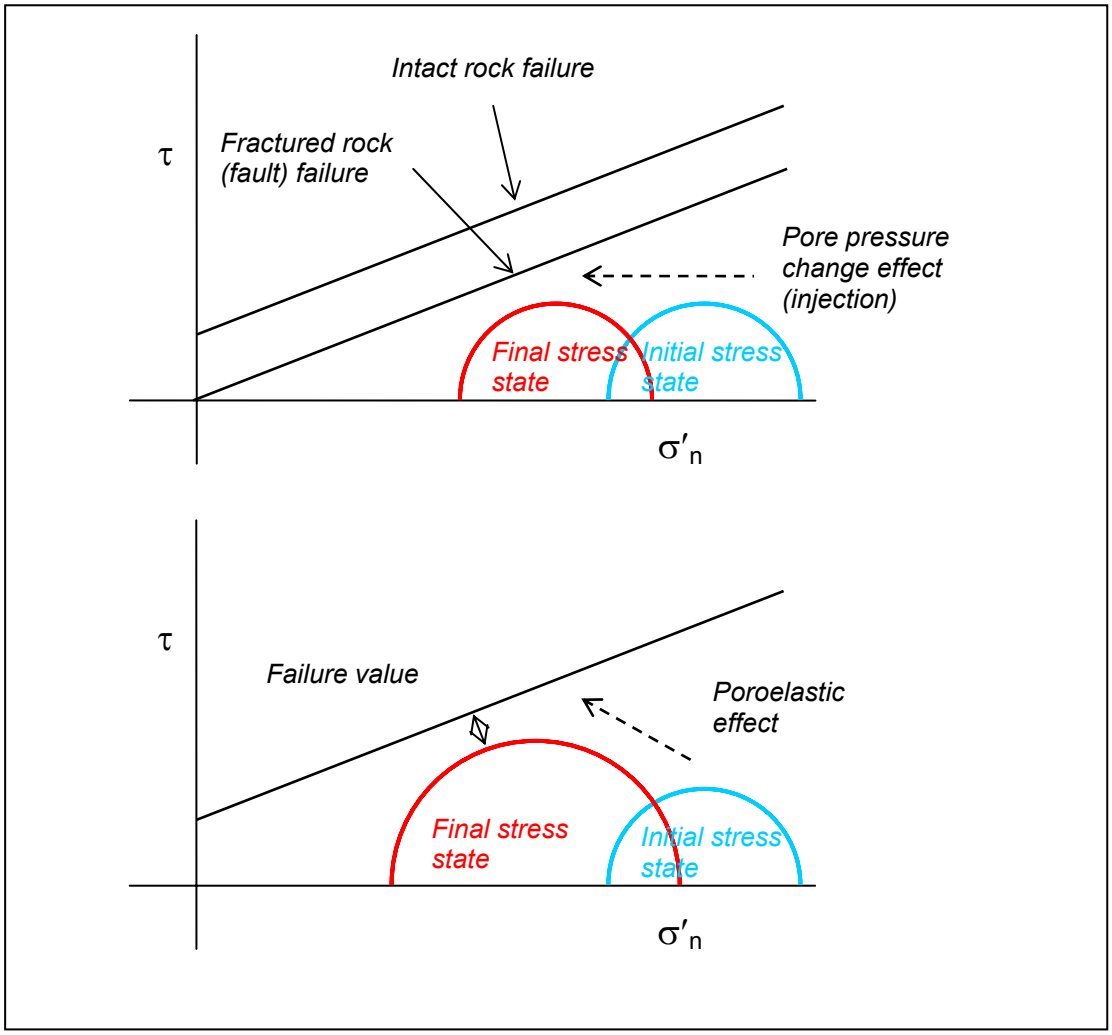

Figure A2.2: Illustrations of Mohr-Coulomb stress states for failure of intact rock

Aquifer name	Unit No.	Maximum CO_2 injection rate (Mt/yr)	Total CO_2 injected in 50 years (Mt)
Findhorn	174	1.5	75
Lossiehead	19	0.6	30
Hopeman_012	71	0.3	15
Orcadia_013	168	0.15	7.5
Alness_012	205	0.04	2

Table A2.5: Maximum injection rates and total CO2 injected determined by geomechanical modelling using trial and error

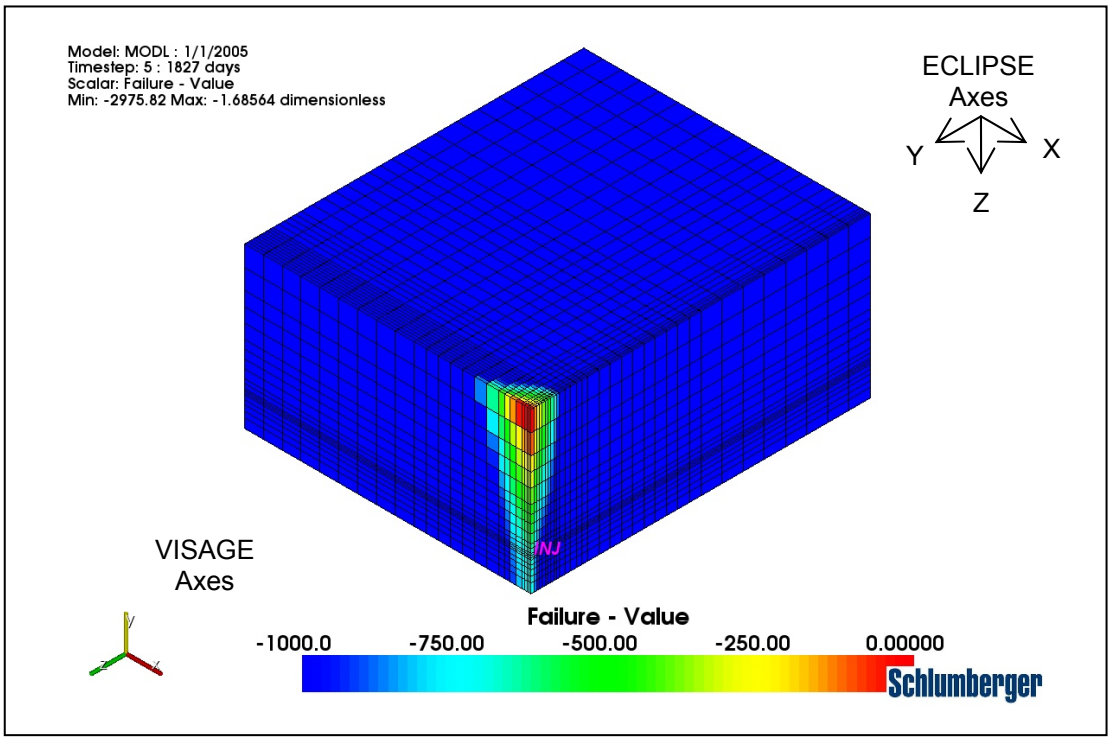

Figure A2.3: Plot of failure value for geomechanical model of LOA Unit 19 without over- and under-burden at time 5 years with 0.7 Mt/yr CO_2 injection rate. (Note, model cut in half along horizontal well trajectory to aid visualization.)

2.4 Effect of Over- and Under-burden

In order to investigate the effect of including an over- and under-burden on the geomechanical modelling, the Eclipse input data for Unit 19 was re-imported into Modeler and re-edited to include "embedding". The embedding extended the model by 5 layers upwards and downwards with an overall thickness of 200 m in each direction. The over-burden layers were of uniform thickness (40 m) but the under-burden layer thicknesses increased geometrically away from the aquifer. No side-burden was modelled.

The same geomechanical properties were used for the over- and under-burden material as the aquifer with the exception that the material was set to purely elastic by setting the Mohr-Coulomb cohesion to a very large number. The same trial and error procedure described above was then used to determine the maximum injection rate. In this case the maximum injection rate was determined as 1.55 Mt/yr. This may be compared to the value of 0.6 Mt/yr for the corresponding model without over- and under-burden.

It is also instructive to compare the location where the material in the model fails. A typical plot of failure value for this model is shown in **Figure A2.4**. It can be seen that failure predominantly occurs at the wellbore location, whereas in the case of no over- and under-burden, failure occurs at the top of the aquifer. This is primarily due to the deformation constraint provided by the material of the over-burden.

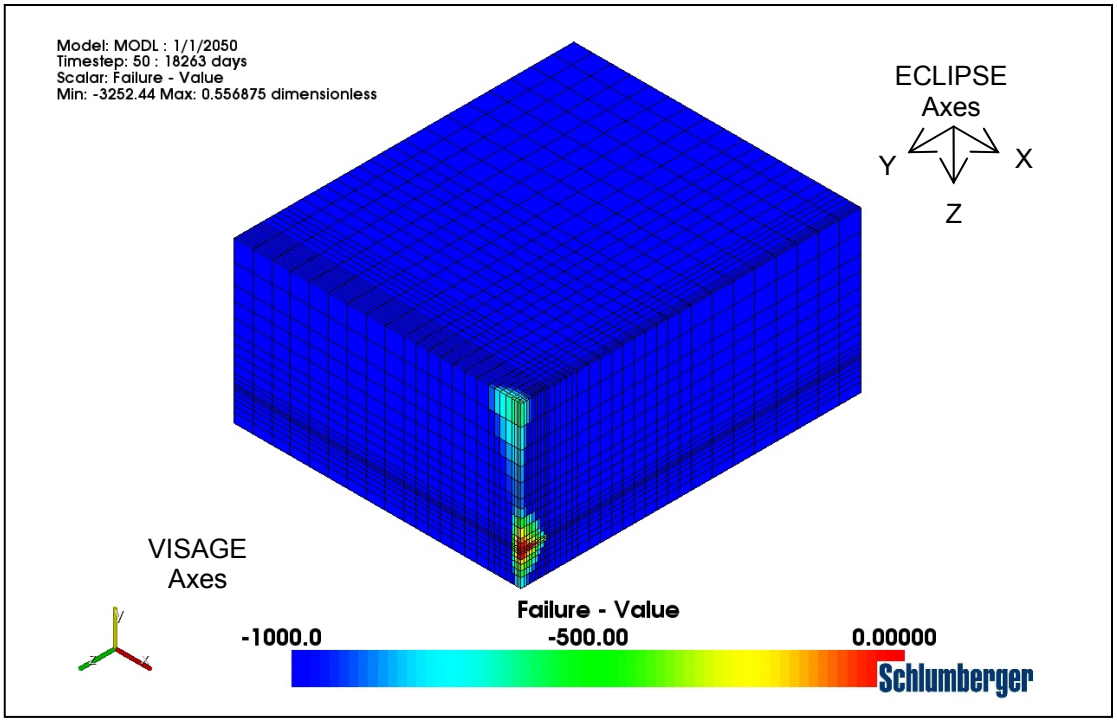

Figure A2.4: Plot of failure value for geomechanical model of LOA Unit 19 with over- and under-burden at time 50 years with 1.6 Mt/yr CO_2 injection rate. (Note, model cut in half along horizontal well trajectory to aid visualization.)

2.5 Conclusions

The geomechanical modelling of low permeability large open aquifer Representative Structures confirmed the low storage capacity estimates made by other dynamic modelling. It was noted however that the effect of including an over- and under-burden in the geomechanical model, could significantly increase the storage capacity estimate and change the location of geomechanical failure.

3 Specific Modelling: Exemplar 1 (Forties)

3.1 Development of Reservoir Simulation Models

The reservoir simulation model for geomechanical injectivity calculations was developed from the Exemplar 1 (Forties) Petrel model produced by Senergy for the project [Long, 2011]. This model is shown in **Figure A3.1**. In order to make more effective use of the Petrel data for geomechanical modelling, a sub-model was developed which covered a reduced areal extent, reconfigured the grid spacing and reduced the number of reservoir layers. The sub-model was based on a rectangular area 10 × 10 km in the middle of the Forties area of interest with a "tartan" grid having a central grid resolution 100 × 100 m, increasing to a 700 m grid at the edges. The number of layers in the model was reduced from 90 in the original Petrel model to 30 in the reservoir sub-model in two different up-scaling scenarios – see below. The sub-model grid dimensions were 47 × 47 × 30 (66,270 cells) as compared to the Senergy Petrel model 180 × 107 × 90 (1,733,400 cells). The reservoir model was based on an ECLIPSE 100 simulation with the aquifer brine modelled as black oil (oil, gas, dissolved gas and vaporized oil present).

The porosity and permeability data for the sub-model was based on two different upscaling scenarios of the original Petrel data (200 × 200 m grid cells). In the first scenario the upscaling was based on porosity and permeability derived from the logs of two wells located within the model area. The facies from these well logs was upscaled preserving the 20:80 shale/sand proportions as in the original Senergy model. The result of this upscaling is illustrated in **Figure A3.2**. The second scenario was based on an upscaling derived directly from the original Senergy model distributions. In this case the facies distribution was effectively "lost" and the shale/sand proportions changed to approximately 10:90. The upscaled Petrel models were then used to generate GRID section data for the ECLIPSE 100 models, together with SATNUM relative permeability regions based on absolute permeability cell data according to project recommendations [RPS Energy, 2010].

The ECLIPSE 100 simulation model was further developed using the best currently available data. This data is summarized in **Table A3.1**. Plots of the general appearance of the reservoir simulation model are shown in **Figure A3.3**. Typical simulation results from the model are illustrated by the fence diagrams shown in **Figure A3.4**. It can be seen here that the gas saturation distribution and pressure response is significantly influenced by the presence of the low permeability (shale) cells.

3.2 Development of Geomechanical Models

Once the reservoir simulation model was working satisfactorily the geomechanical model data was developed first by importing the ECLIPSE 100 input data into the VISAGE software [Schlumberger, 2009]. The input data was imported into the Modeler where it was conditioned for the geomechanical modelling. This consisted of the embedding of the model (reservoir) with an overburden and underburden and the assignment of rock mechanical properties to the various parts of the model.

The reservoir was embedded by the addition of approximately 600 m of material to the top and bottom in 10 layers with a geometric increase in layer thicknesses away from the reservoir layers. No side-burden embedding was made. The general appearance of the geomechanical model grid is shown in **Figure A3.5**.

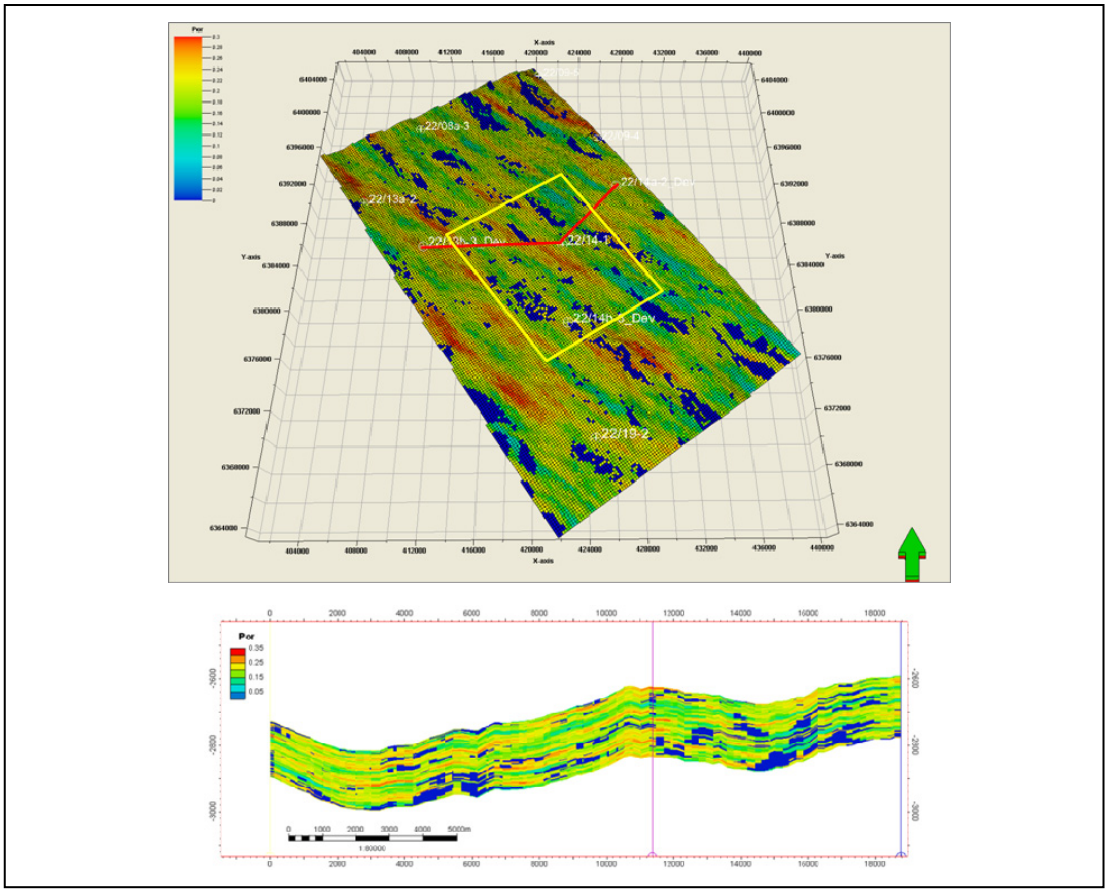

Figure A3.1: Senergy Forties Petrel model showing porosity distribution – the red line is the path of the section profile shown in the lower figure and the yellow rectangle indicates area selected for the geomechanical sub-model.

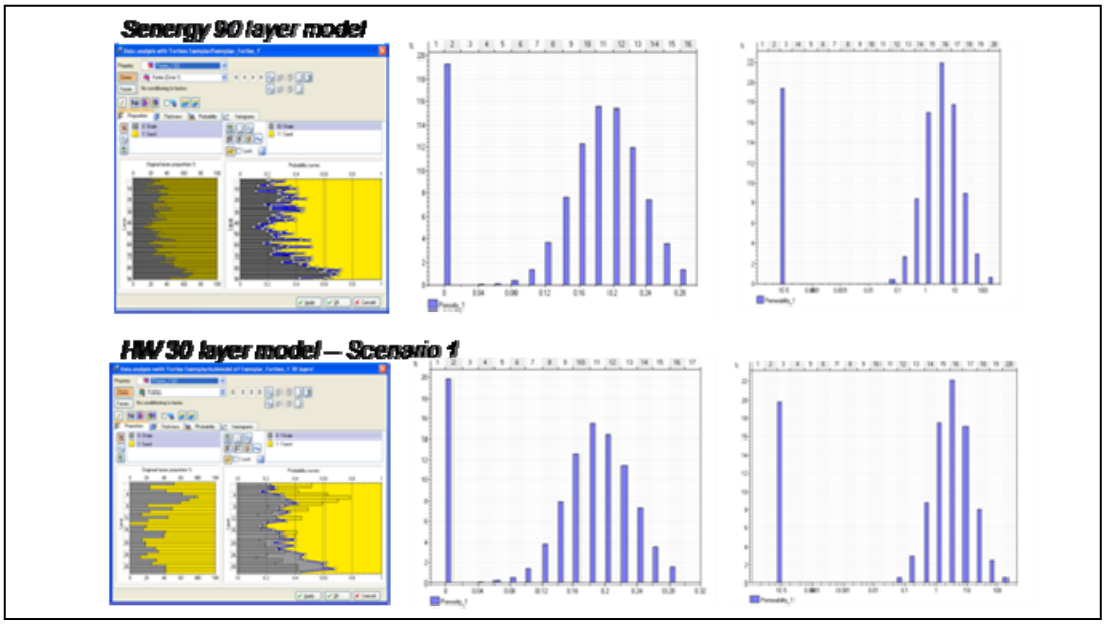

Figure A3.2: Comparison of facies, porosity and permeability distributions in original Senergy Petrel model and sub-model developed for geomechanical simulation

Data section etc.	Specification	Data source
~RUNSPEC		
Dimensions	47 × 47 × 30 (66,270 cells)	
Fluids/ phases	OIL, GAS, DISGAS, VAPOIL	
Units	METRIC	
~GRID		
Geometry	10 km × 10 km sub-model in middle of AOI Tartan grid, 100 m × 100 m cells in central region 700 m × 700 m cells at edge corners	
Porosity & permeability	Based on upscaling of Senergy Petrel model Zero permeability values replaced by 1.0E-5 PERMX = PERMY, PERMZ multiplied by 0.1	
Boundary conditions	Porosity multiplier ×50 applied to all edge cells	
~PROPS		
Fluid saturation functions	No imbibition/hysteresis data used as only modelling injection phase.	RPS data on sharepoint.
PVT data	Black Oil data assuming reservoir temperature of 100°C and salinity of 100,000 ppm (PVT_T_100_S_100000ppm.inc).	RPS data on sharepoint
Rock compressibility	5.8×10^{-5} bar^{-1} at 305.3 bar	
~REGIONS		
Saturation regions	4 SATNUM regions applied according to permeability: 1. < 0.1 mD (Calmar – shale) 2. 0.1 to < 10 mD (Viking 1) 3. 10 mD to 100 mD (Viking2) 4. > 100 mD (Berea)	RPS data on sharepoint
~SOLUTION		
Equilibration	Pore pressure gradient calculated according to brine density in PVT_T_100_S_100000ppm.inc 273.2 bar at datum depth 2,600 m Oil-water-contact at 10,000 m depth Dissolved gas-oil and vaporized oil-gas ratio assumed zero over depth interval 1,000 to 4,000 m	
~SCHEDULE		
Well(s)	Single vertical well completed throughout all layers kh values range from ~1000 to ~6000 mD m depending on well location. Also used a predefined kh of 10,000 mD m BHP limit 600 bar	
Injection rates	0.5 to 4.5 Mt/yr[4]	
Time steps	Various up to 1000 days and 50 years	

Table A3.1: Reservoir simulation input data for geomechanical sub-model of Exemplar 1 (Forties)

[4] CO_2 density of 1.88 kg/m^3 assumed at surface, 1 Mt/yr equivalent to 1456304 sm^3/day

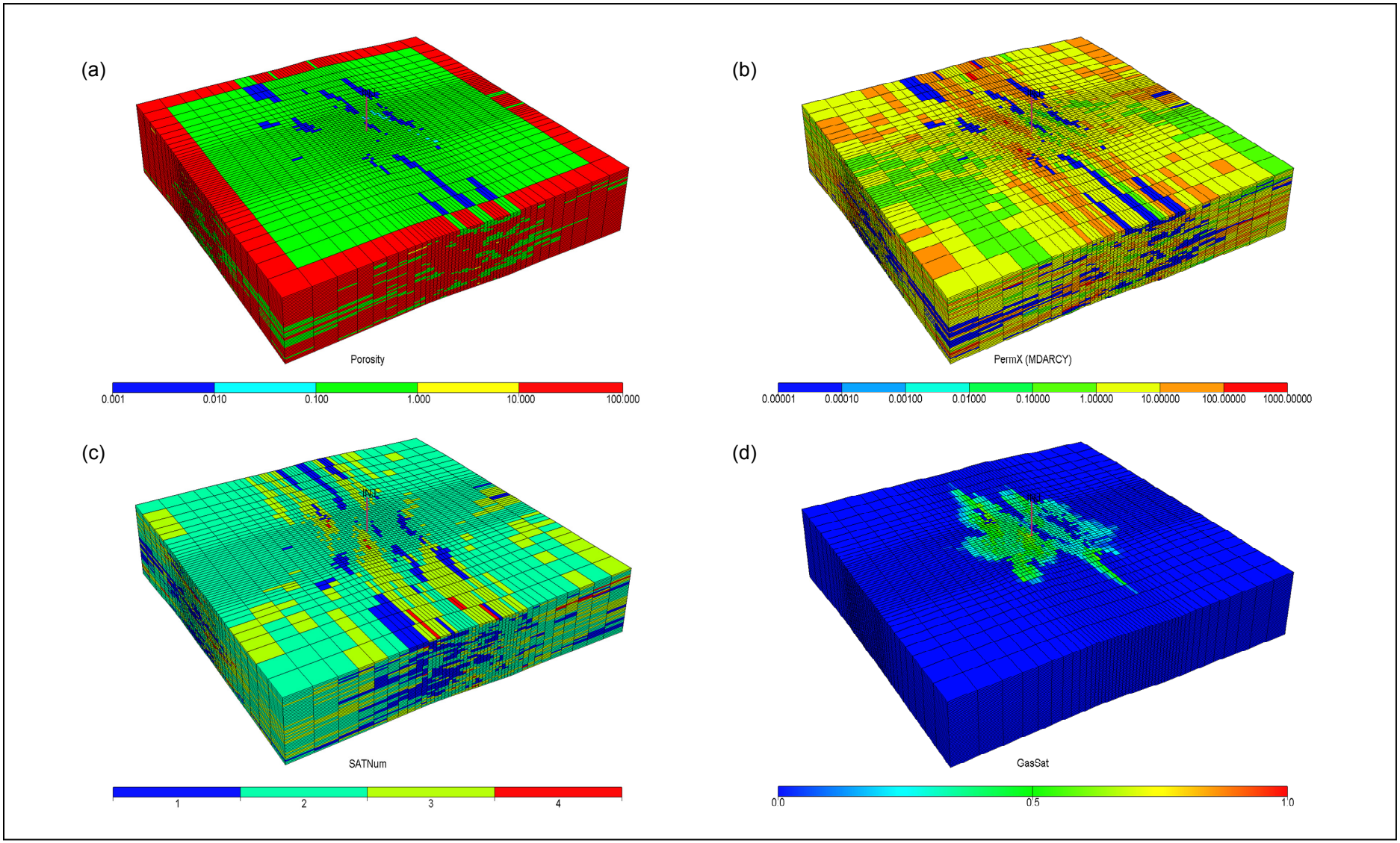

Figure A3.3: General views of Exemplar 1 (Forties) reservoir simulation sub-model developed for geomechanical modelling: (a) porosity distribution, (b) permeability distribution, (c) saturation function (relative permeability) number and (d) gas saturation at end of injection

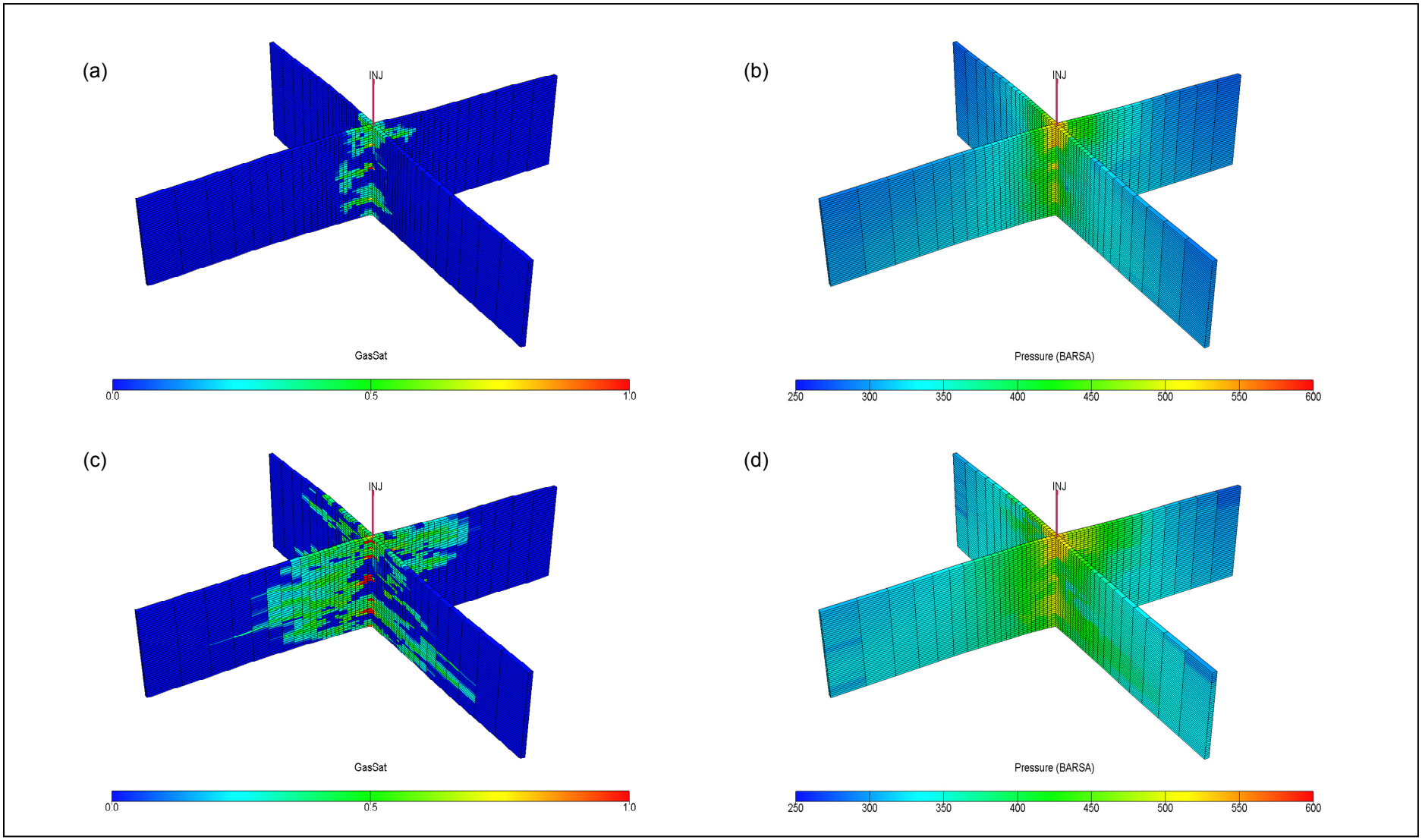

Figure A3.4: Fence diagrams showing typical reservoir simulation results from Exemplar 1 (Forties) reservoir simulation sub-model developed for geomechanical modelling: (a) gas saturation after 5 years injection, (b) pore pressure after 5 years injection, (c) gas saturation at end of injection and (d) pore pressure at end of injection.

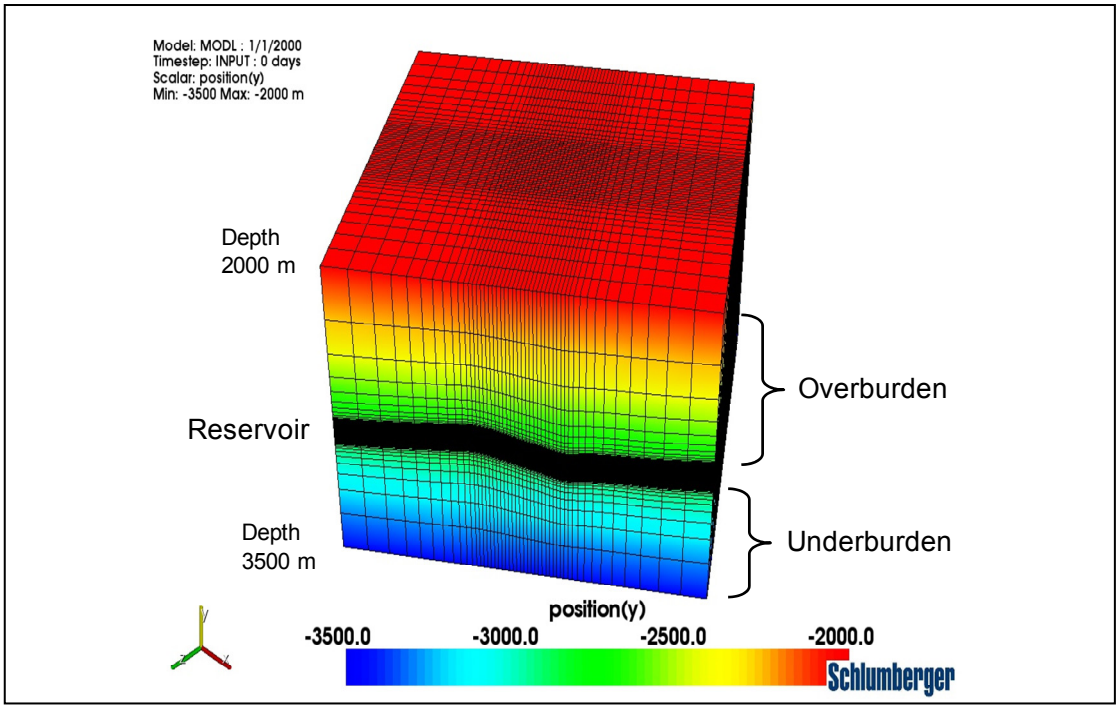

Figure A3.5: General appearance of Exemplar 1 (Forties) geomechanical model

Geomechanical property	Reservoir	Over/under burden
Elastic		
Young's modulus GPa	2.0	2.0
Poisson's ratio	0.2	0.2
Biot's coefficient	1.0	1.0
Non-linear		
Mohr-Coulomb failure criterion		
Cohesion kPa	100	~∞
Angle of internal friction °	30	n/a
Dilation angle °	5	n/a
Tensile cut-off	~∞	n/a
Fluidity parameter	1.0	n/a
Hardening parameter	0.0	n/a
Initialisation		
Total vertical stress gradient kPa/m	22.44	22.44
Additional vertical stress kPa	0.0	0.0
Maximum horizontal stress coefficient	0.8	0.8
Minimum horizontal stress coefficient	0.8	0.8
Horizontal stress azimuth °	-35.0	-35.0
Vertical stress inclination °	90.0	90.0
Pore pressure gradient kPa/m	10.0	10.0
Additional pore pressure kPa	0.0	0.0

Table A3.2: Geomechanical properties initially used in the Exemplar 1 (Forties) geomechanical model

Geomechanical properties were assigned to the model as given in **Table A3.2**. Essentially the model was assumed to be composed of material with uniform geomechanical properties with reservoir only having inelastic (failure) properties – a basic Mohr-Coulomb failure criterion with very conservative failure parameters assumed.

The geomechanical model data was then exported from the VISAGE Modeler so that it could be run in coupled with the reservoir simulation model. Again, the model was run without porosity or permeability updating i.e. so that the pressure changes from the ECLIPSE simulation were only used to modify the stress/strain state through changes in effective stress, and there was no feedback to the flow model. Various configurations of the model were run with changes in well orientation, injectivity (Kh) value, CO_2 injection rate, in situ horizontal to vertical stress ratio and internal angle of friction, as summarised in **Table A3.3**. As previously, the results of the simulation were reviewed to identify if failure had occurred in the geomechanical model as indicated by a zero/near zero failure value (shear failure). Typical observed shear failure results are presented in **Figure A3.6**.

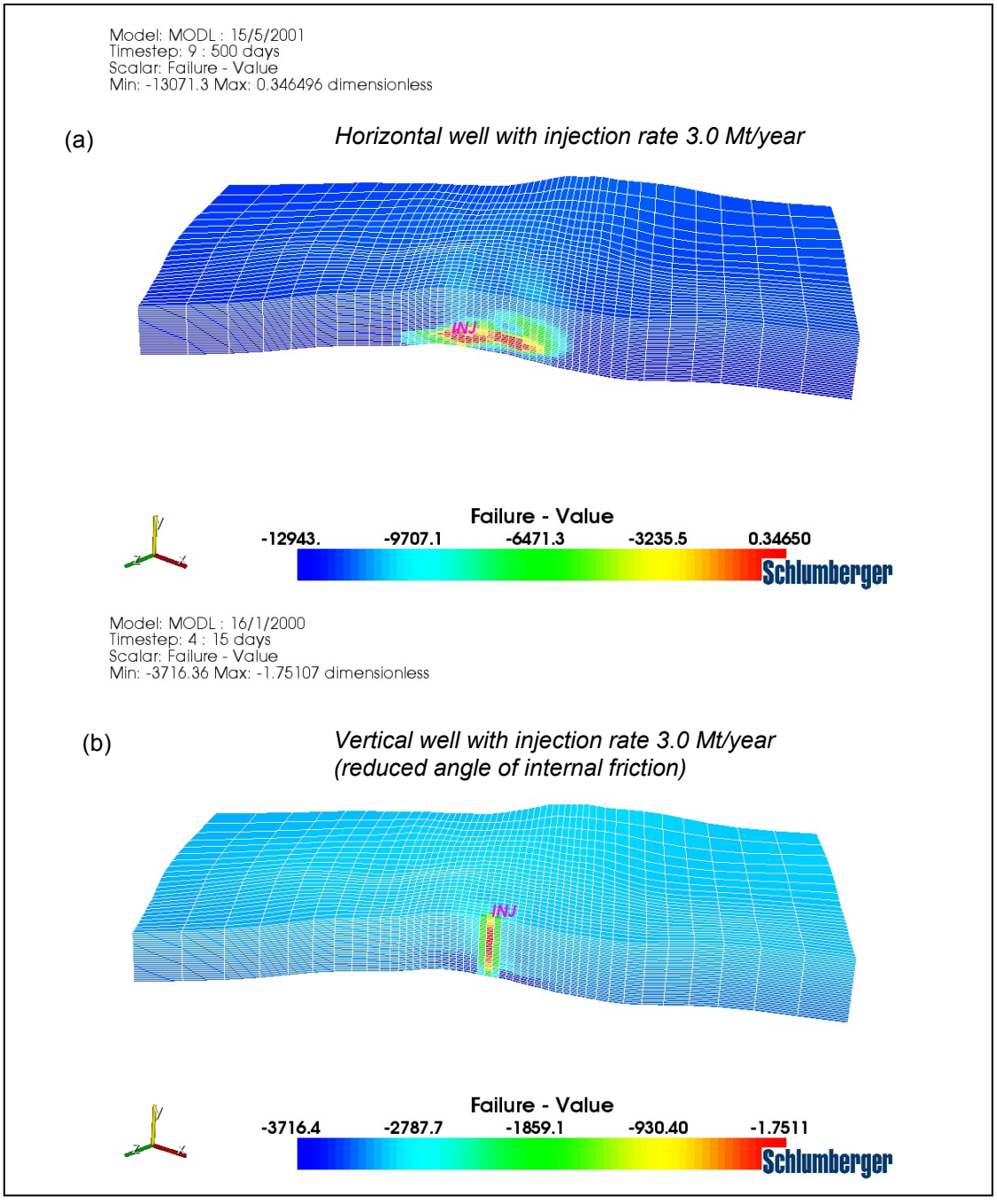

Figure A3.6: Typical shear failure results for Exemplar 1 (Forties) geomechanical model: (a) horizontal well and (b) vertical well. Note model cut away to well location and small near negative values indicate failure.

3.3 Results

The simulation results are presented graphically in **Figure A3.7** where the well bottom hole pressure (WBHP) has been plotted against time for the various cases together with observations about proximity to failure in **Table A3.3**.

I/D	Geological scenario	Well orientation	Kh mD m	Injection rate Mt/year	S_h/S_v	Φ °	Proximity to failure	Location
a	1	Vertical	1,054	0.75	0.8	30	No failure, FV[5] -5238 kPa at 15 days	
b	1	Horizontal	10,629	3.0	0.7	30	No failure, FV -1512 kPa at 2 days	Initially at wellbore, then aquifer top
c	1	Horizontal	10,629	3.0	0.8	30	No failure, FV -343 kPa at 1000 days	At wellbore
d	1	Horizontal	10,629	3.0	0.9	30	Failure at 500 days	At wellbore
e	1	Horizontal	10,629	3.0	1.0	30	Failure at 100 days	At wellbore
f	2	Vertical	*10,000*	3.0	0.9	30	No failure, FV -7424 kPa at 15 days	
g	2	Vertical	*10,000*	4.5	0.8	30	No failure, FV -628 kPa at 15 days	
h	2	Vertical	*10,000*	4.5	0.8	20	Failure at 2 days	
i	2	Vertical	*10,000*	3.0	0.8	20	Near failure, FV -1.75 kPa at 15 days	

Table A3.3: Summary of Exemplar 1 (Forties) geomechanical modelling input parameters and results

The initial model with a vertical well (case a) had low injectivity (1,054 mD m) and the maximum injection rate that could be achieved without the WBHP pressure exceeding 600 bar was 0.75 Mt/year. Even at this injection rate no failure was detected. The well orientation was changed to horizontal (1 km length) and the injectivity increased to 10,629 mD m. Higher injection rates could then be achieved without exceeding the 600 bar limit. For the case of Sh/Sv = 0.8 (case c) at 3.0 Mt/year injection rate again no failure was observed. However for higher values of Sh/Sv (cases d and e) failure was observed at 500 and 100 days respectively. For the case of Sh/Sv = 0.7 (case b) no failure was observed but the trend was seen that the proximity to failure was even greater than case c.

For the second set of scenarios the well was returned to a vertical orientation (as expected to be utilized in the Exemplar 1 full-field dynamic modelling) but the injectivity of the reservoir layers was explicitly specified rather than being derived by ECLIPSE from the well penetrated cell properties. In these cases (f to i) the well Kh was set to 10,000 mD m. The higher Kh values enabled a higher injection rate to be examined – case g (4.5 Mt/year) compared to case f (3.0 Mt/year), but failure/near failure was not observed until the internal angle of friction has reduced from 30° to 20° (cases h and i).

[5] FV indicates “failure value”

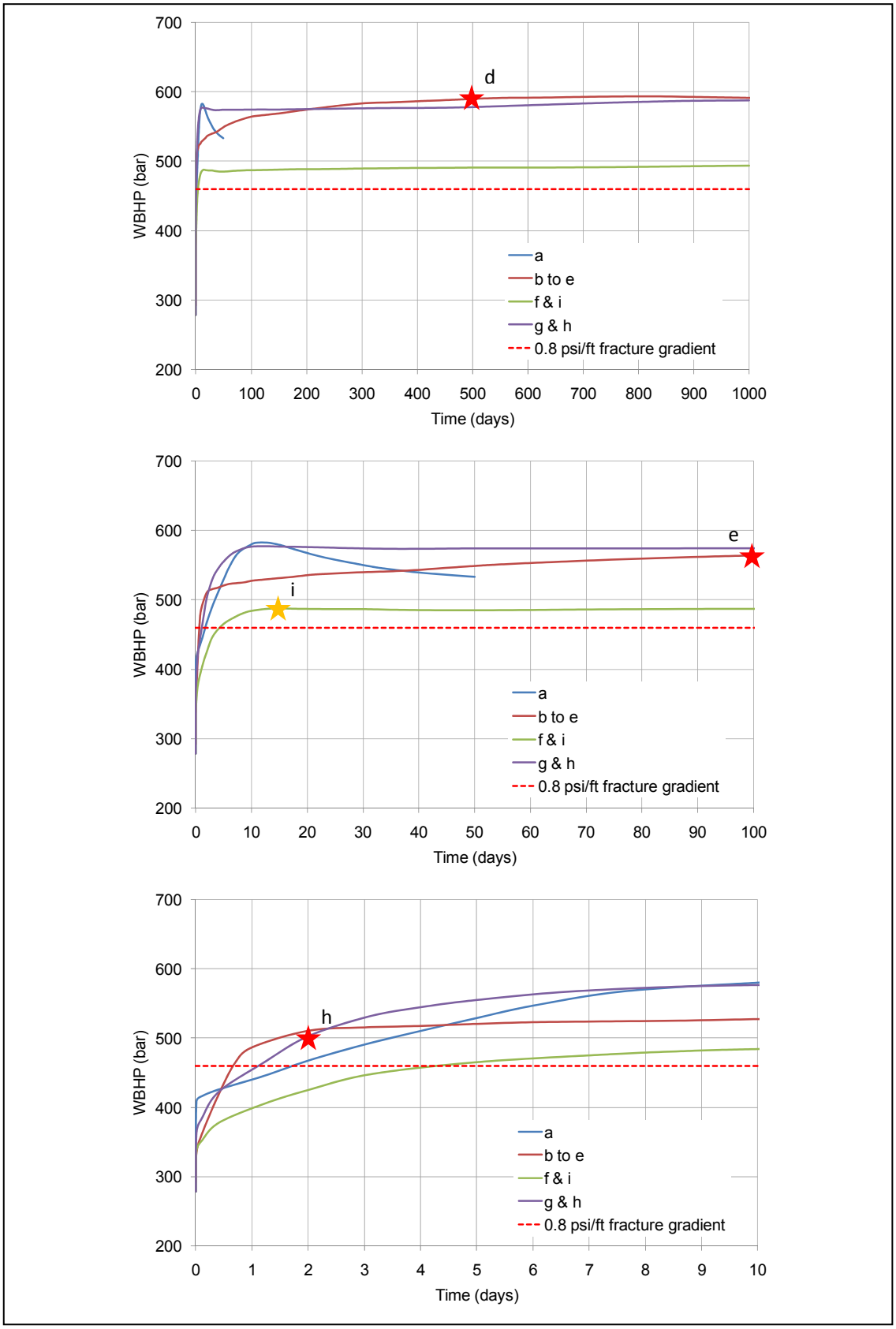

Figure A3.7: Plots of injector bottom hole pressure versus time for the various cases of the Exemplar 1 (Forties) geomechanical model annotated with shear failure events – red stars indicate failure and yellow star near failure. Note each graph shows the same WBHP data but with the time axis range changed

3.4 Hydraulic Fracturing and Fault Reactivation Potential

Besides the geomechanical failure by shear failure of the intact rock with the injection of CO_2, there also exists the possibility of failure by hydraulic fracturing or the reactivation of existing fracture of faults. Both modes of failure can lead to CO_2 leakage from the aquifer formation and compromise the integrity of the geological storage.

A simple criterion for hydraulic fracturing is to assume failure occurs when the minimum principal effective stress σ'_3 is zero (also assumes a rock tensile strength of zero), whilst in theory hydraulic fracturing failure can be represented by a geomechanical model, because it is essentially a wellbore phenomenon where tensile stresses can be generated, it cannot be captured by a reservoir scale model where there is inadequate grid resolution at the well location. The alternative used in the project then to assess geomechanical failure by hydraulic fracture at the wellbore by the calculation of a safe injection pressure based on a fracture pressure gradient e.g. 90% of pressure at a particular depth assuming a gradient of say 0.8 psi/ft derived from empirical measurements from leak-off tests.

The reactivation of existing fractures and faults can also be investigated by geomechanical modelling. A simple criterion for fault (fracture) reactivation through shear slip can be derived from the Mohr-Coulomb criterion [Rutqvist & Tsang, 2002]. For cohesion-less faults with a coefficient of friction of 0.6 (field observation lower value) this can be expressed as:

$$\sigma'_1 = 3\sigma'_3$$

i.e. shear slip would be induced wherever or whenever the maximum principal effective stress σ'_1 exceeds three times the minimum principal effective stress σ'_3 on preferentially orientated faults. This criterion is very similar to that for the shear failure of intact rock here where a very low value of cohesion (100 kPa) has been assumed and the angle of internal friction is taken as 30°.

Plots of the minimum principal effective stress σ'_3[6] as an indicator of hydraulic fracturing together with the (shear) failure value and the calculated ratio $\sigma'_1/3\sigma'_3$ are shown in **Figure A3.8 and Figure A3.9** for the cases of a horizontal well and vertical well respectively. For the minimum principal effective stress (a) it can be seen that in both cases the maximum (least negative) is more than -5000 kPa at the wellbore location indicating that the models are not near predicting failure by hydraulic fracturing. For the fault (fracture) reactivation calculation (c) – where the critical value is unity – it can be seen that it closely follows the shear failure value (b) – where the critical value is zero.

The observation from these results is that for the geomechanical models developed and the geomechanical property data assumed here, the (shear) failure value results will be a close proxy for the potential of fault reactivation, whilst the potential for hydraulic fracturing cannot be adequately assessed.

[6] Note because VISAGE stress convention is compression negative, the minimum principal stress in displayed as “p1” in Modeler.

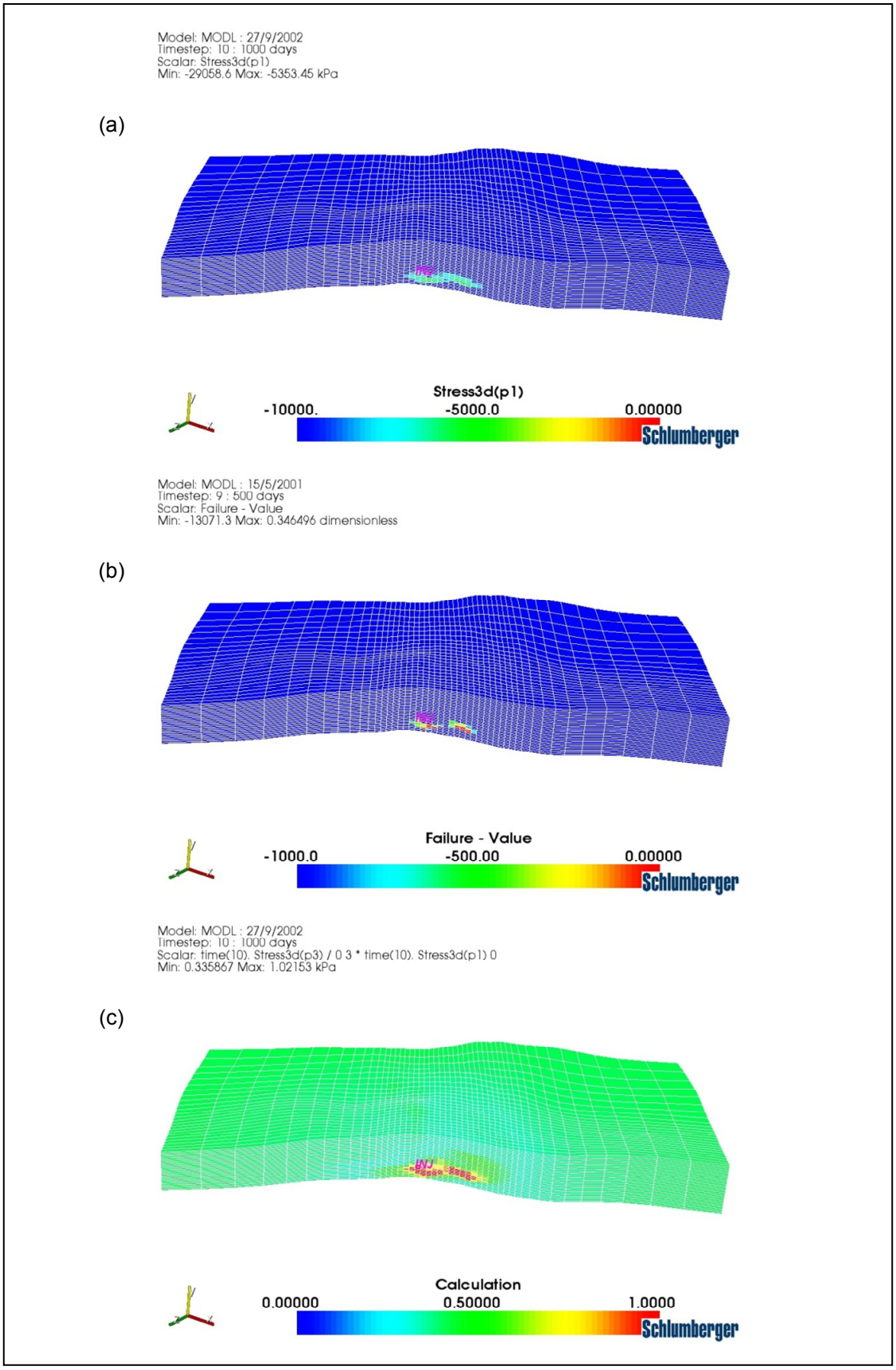

Figure A3.8: Plots of (a) minimum principal effective stress σ'_3, (b) failure value and (c) calculation $\sigma'_1/3\sigma'_3$ for typical case of a horizontal well

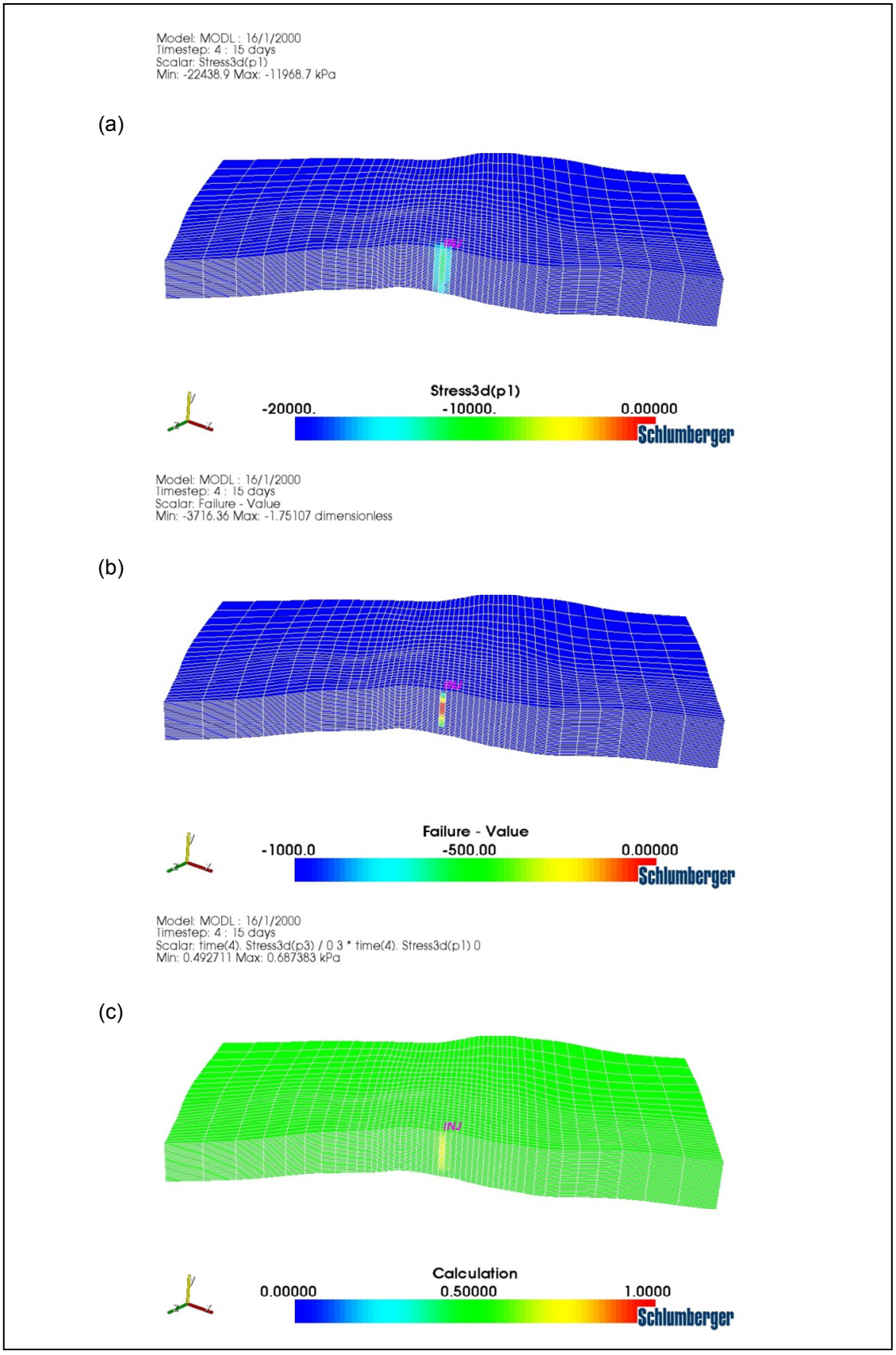

Figure A3.9: Plots of (a) minimum principal effective stress σ'_3, (b) failure value and (c) calculation $\sigma'_1/3\sigma'_3$ for typical case of a vertical well

4 Leak-off Test Data/fracture Pressure Gradient Sensitivity Study

In order to assess the sensitivity of well injectivity and storage capacity to fracture pressure gradient a small study was carried out just using the reservoir simulation sub-model of Exemplar 1 without the coupled geomechanical modelling. As a preliminary, leak-off pressure test data for a number of wells in the Forties area of interest was examined[7]. The pressure tests comprised data from both leak-off (LOP-LO) and limit (LOP-LT) tests. A screenshot from the pressure data visualisation software is also shown in **Figure A4.1** where each test value is plotted against depth (TVDss) for the wells.

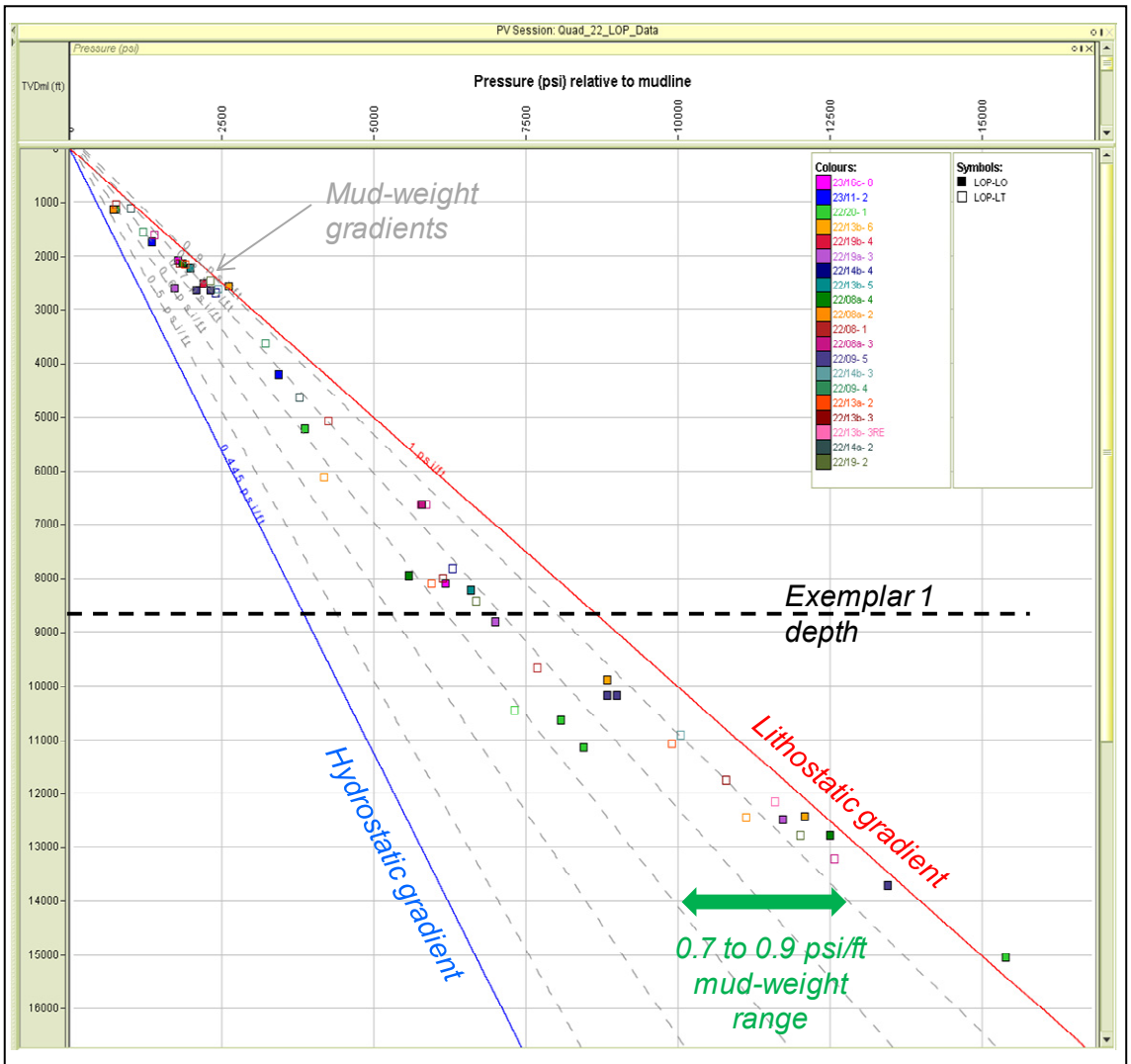

Exemplar Wells		Additional Wells		
22/8a-3 (v)	22/19-2 (v)	22/8-1	22/19a-3	23/16c-8
22/9-4 (v)	22/15-1 (v)	22/8a-2	22/19b-4	22/15-1
22/9-5 (v)	22/13b-3 (Dev)	22/8a-4	22/13b-6	
22/13a-2 (v)	22/14a-2 (Dev)	22/13b-5	22/20-1	
22/14-1 (v)	22/14b-3 (Dev)	22/14b-4	23/11-2	

Figure A4.1: Leak-off pressure test data from Forties AOI wells

[7] Data provided by GeoPressure Technology Ltd.

Although the data in **Figure A4.1** is sparse it illustrates that there is a range of fracture pressure gradients within the wells ranging from 0.6 psi/ft to nearly 1 psi/ft with an average of around 0.8 psi/ft. Interestingly there is a general change in the trend with higher pressures observed below 10,000 ft which is typically observed in the Central North Sea province. However from the data, at the Exemplar 1 depth, the fracture pressure gradient may generally be taken to lie within the range 0.7 to 0.9 psi/ft.

Using the geological scenario 2 ECLIPSE 100 model the location of a vertical well was varied about the central 5 × 5 (100m) cells of the grid calculating the total layer Kh values for each well. Three vertical well locations were then chosen which had Kh values corresponding to 1,042 (Low), 3,445 (Average) and 5,995 (High) mD m. The edge cell pore volume multiplier applied was set at ×50 and the model run at the three different well locations with the well BHP controlled to 90% of the fracture pressure for gradients 0.7, 0.8 and 0.9 psi/ft. The injection period was 50 years.

Using the average Kh well, the model was also run varying the edge cell pore volume multiplier over the range ×20 to ×5000 corresponding to the equivalent boundary distances given in **Table A4.1**.

PVMULT	Distance (km)
20	12
50	19
100	26
5000	180

Table A4.1: Aquifer equivalent boundary distances for different model edge PV multipliers

The total CO_2 injected over a 50 year period was calculated and the results are presented graphically in **Figure A4.2**.

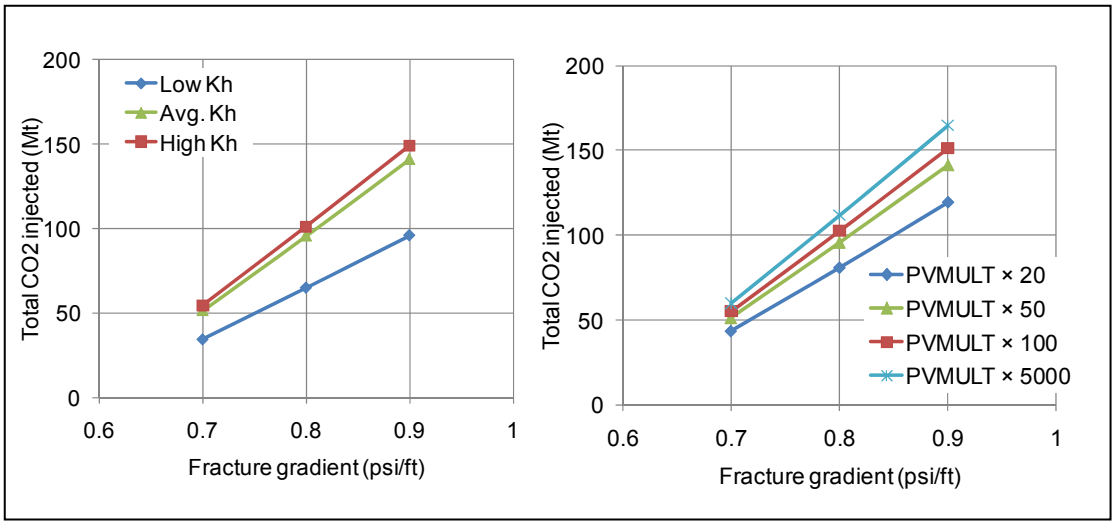

Figure A4.2: Sensitivity of total CO2 injected to fracture pressure gradient for various well injectivity Kh values and aquifer extent (model edge PV multiplier)

It can be seen from the results that there is significant sensitivity in the total amount of CO_2 injected to the fracture pressure gradient. A small change in the gradient value e.g. 0.05 psi/ft

(~6%) can lead to a 20 to 25 Mt change in the amount injected in 50 years. This sensitivity is nearly independent of the equivalent extent of the aquifer.

5 Conclusions

The coupled geomechanical models of representative structures of low permeability large open aquifers used to determine maximum injection rates without geomechanical failure, gave total CO_2 storage capacities very similar to those obtained by assuming a maximum injection pressure 90% of fracture pressure (taking a fracture gradient of 0.8 psi/ft). These models however did not include the effects of an over-and underburden. With this latter feature included the maximum injection rate without geomechanical failure was seen to significantly increase, with the location of geomechanical failure moving from the aquifer top to the wellbore.

For the coupled geomechanical Exemplar model which also included an over- and underburden, geomechanical failure, when it occurred, was always observed at well bottom hole pressures greater than that which would be predicted by the fracture pressure gradient. This discrepancy in the modelling may be accounted for by the model which did not adequately represent the near wellbore and could not simulate hydraulic fracturing because the gridding was unsuitable. Although hydraulic fracturing remote from the wellbore, shear failure of the intact rock and by proxy reactivation of faults and fractures was captured, the fracture pressure gradient was considered to be the most conservative criterion for injectivity avoiding geomechanical failure.

A supplementary non-geomechanical study showed that pressure constrained injection estimates were very sensitive to the magnitude of the fracture pressure gradient.

6 References

1. VISAGE System & VISAGE Modeler User's Guides. Schlumberger, 2009.
2. Representative Structure Modelling of Dipping Open Saline Aquifers. Appendix 3 of Final Project Report. Prepared by RPS Energy for ETI, June 2011
3. Long, K. Forties Exemplar Static Model Update. Senergy Geologist presentation at WP4 technical meeting held at Imperial College, London 13 January 2011.
4. Approach for Dynamic Modelling of CO2 Storage in Deep Saline Aquifers. Technical report prepared by RPS Energy for ETI, March 2010.
5. Rutqvist, J. and Tsang, C.F. A study of caprock hydromechanical changes associated with CO2 injection into a brine formation. Environmental Geology, 42: p. 296-305, 2002.